A refined ring polymer molecular dynamics theory of chemical reaction rates

Ian R. Craig and David E. Manolopoulos

Physical and Theoretical Chemistry Laboratory,

Oxford University, South Parks Road, Oxford OX1 3QZ, UK

Abstract

We further develop the ring polymer molecular dynamics (RPMD) method for calculating chemical reaction rates [I. R. Craig and D. E. Manolopoulos, J. Chem. Phys. **122**, 084106 (2005)]. We begin by showing how the rate coefficient we obtained before can be calculated in a more efficient way by considering the side functions of the ring-polymer centroids, rather than averaging over the side functions of the individual ring-polymer beads. This has two distinct advantages. First, the statistics of the phase space average over the ring-polymer coordinates and momenta are greatly improved. Second, the resulting flux-side correlation function converges to its long-time limit much more rapidly. Indeed the short-time limit of this flux-side correlation function already provides a "quantum transition state theory" (QTST) approximation to the final rate coefficient. In cases where transition state recrossing effects are negligible, and the transition state dividing surface is put in the right place, the RPMD rate is therefore obtained almost instantly. We then go on to show that the long-time limit of the new flux-side correlation function, and hence the fully converged RPMD reaction rate, is rigorously independent of the choice of the transition state dividing surface. This is especially significant because the optimum dividing surface can often be very difficult to determine for reactions in complex chemical systems.

I. INTRODUCTION

There is considerable current interest in the theory of chemical reaction rates in complex systems (in liquids, on surfaces, and in proteins). A number of different methods have been suggested for computing these rates, ranging from classical trajectory based techniques such as centroid molecular dynamics[1–5] and the classical Wigner model[6] to purely statistical ("quantum transition state theory"[7–19]) type techniques such as the quantum instanton (QI) model.[20–26] The rationale behind these latter techniques is that transition state recrossing effects are unlikely to be very significant in complex systems.[27] Indeed the QI model has recently been shown to give satisfactory results for a variety of problems, ranging from the gas phase $H+CH_4$ reaction[23] to a model for a chemical reaction in a polar solvent.[25] In all of the problems to which it has so far been applied, however, it has been fairly straightforward to determine a good choice for the transition state dividing surface. It is not at all clear that this will always be the case for reactions in complex systems, and since the accuracy of the QI model depends crucially on the choice of dividing surface the development of alternative techniques is certainly desirable.

In a series of recent papers,[28–31] we have shown how the standard path-integral molecular dynamics method,[32] which has been used for the last twenty years to compute the static equilibrium properties of quantum mechanical systems, can be generalized to calculate approximate Kubo-transformed real-time correlation functions,[33] and so applied to the study of chemical dynamics. The resulting correlation functions are exact in the limit as $t \to 0$, consistent with the quantum mechanical time-reversal and detailed-balance symmetries, and in the special case where one or other of the correlated operators is a linear function of the coordinates or momenta they give the exact result for a harmonic potential.[28] So far, this ring polymer molecular dynamics (RPMD) method has been applied to a simple model for chemical reaction in solution and to the deep tunneling through a one-dimensional Eckart barrier,[29] and to the diffusion in[30] and the inelastic neutron scattering from[31] a strongly quantum liquid (*para*-hydrogen). Overall, the results of these applications have been quite encouraging, and they suggest that the method provides a rather promising way to include quantum statistical effects in condensed phase molecular dynamics.

In the present paper, we return to the RPMD calculation of chemical reaction rates, and significantly improve on the formulation of this problem that we gave originally.[28] In

particular, we show that the RPMD rate coefficient can be calculated in a simpler way by correlating the side functions of the ring-polymer centroids rather than averaging over the side functions of the individual ring-polymer beads. We also demonstrate that the theory reduces within this new formulation to the early "quantum transition state theory" (QTST) of Voth, Chandler and Miller[10] in the short-time limit, and that it is rigorously independent of the choice of the transition state dividing surface in the limit as $t \to \infty$. This is a highly desirable feature of the method for the reasons discussed above. While the exact quantum mechanical reaction rate is independent of the choice of dividing surface, and the same is true in the classical limit, it is quite unusual for this feature to be present in an approximate quantum mechanical (or semiclassical) theory. It is not present, for example, in either the classical Wigner model[6] or the QI model,[20–26] which in other respects are two of the more promising methods that have been suggested for calculating chemical reaction rates.

Rather than separate the present theoretical developments from the results that illustrate them, we have found it more convenient in this paper to present the theory and results together in Section II. Throughout most of this section, we have confined our equations and our illustrative example calculations to the simple case of a one-dimensional reaction, to get the points we want to make across as clearly as possible. We should therefore stress from the outset that there is absolutely no difficulty in extending the RPMD equations to multi-dimensional reactions, as we have already shown in our earlier paper:[29] it is simply that the multi-dimensional equations take longer to write down (see Section II.H). The final section (Section III) summarizes what we have accomplished in the present study.

II. THEORY AND RESULTS

A. Reaction rate theory

As we have already mentioned, we shall focus most of our discussion on a simple one-dimensional barrier transmission problem with a Hamiltonian of the form

$$H = \frac{p^2}{2m} + V(q), \tag{1}$$

where the potential $V(q)$ tends to zero as $q \to -\infty$ and to a constant as $q \to \infty$. This provides the simplest possible model for a bimolecular chemical reaction.

According to Miller, Schwartz and Tromp,[34] the exact quantum mechanical rate coefficient for this problem can be written equivalently as

$$k(T) = \frac{1}{Q_r(T)} \int_0^\infty c_{ff}(t)\, dt = \frac{1}{2Q_r(T)} \int_{-\infty}^\infty c_{ff}(t)\, dt, \tag{2a}$$

$$k(T) = \frac{1}{Q_r(T)} \lim_{t\to\infty} c_{fs}(t), \tag{2b}$$

and

$$k(T) = -\frac{1}{Q_r(T)} \lim_{t\to\infty} \frac{d}{dt} c_{ss}(t), \tag{2c}$$

where $Q_r(T)$ is the reactant partition function per unit length and $c_{ff}(t)$, $c_{fs}(t)$ and $c_{ss}(t)$ are flux-flux, flux-side, and side-side correlation functions[34]

$$c_{ff}(t) = \mathrm{tr}\left[e^{-\beta H/2} F e^{-\beta H/2} e^{+iHt/\hbar} F e^{-iHt/\hbar}\right], \tag{3a}$$

$$c_{fs}(t) = \mathrm{tr}\left[e^{-\beta H/2} F e^{-\beta H/2} e^{+iHt/\hbar} h e^{-iHt/\hbar}\right], \tag{3b}$$

and

$$c_{ss}(t) = \mathrm{tr}\left[e^{-\beta H/2} h e^{-\beta H/2} e^{+iHt/\hbar} h e^{-iHt/\hbar}\right], \tag{3c}$$

with $\beta = 1/(k_{\mathrm{B}}T)$, $h = h(q - q^\ddagger)$, and

$$F = \frac{i}{\hbar}\left[H, h\right]. \tag{4}$$

The three equivalent expressions for $k(T)$ in Eq. (2) arise from the fact that the reactive flux operator F in Eq. (4) is the Heisenberg time derivative of the product side operator h; the minus sign in Eq. (2c) comes from the time-reversal symmetry of quantum mechanics and the fact that the side operator that is differentiated on going from $c_{ss}(t)$ to $c_{fs}(t)$ is evaluated at time zero rather than time t.[34]

Although it is not immediately obvious from these equations, the rate $k(T)$ in Eq. (2) is rigorously independent of the location of the dividing surface $q^\ddagger$. This follows because $k(T)Q_r(T)$ can be expressed as a Boltzmann average of a cumulative reaction probability,[35]

$$k(T)Q_r(T) = \frac{1}{2\pi\hbar} \int_{-\infty}^\infty e^{-\beta E} N(E)\, dE, \tag{5}$$

where $N(E)$ is given by Eq. (2a) as[34]

$$N(E) = \frac{1}{2}(2\pi\hbar)^2 \mathrm{tr}\left[F\delta(E-H)F\delta(E-H)\right]. \tag{6}$$

Writing the microcanonical density operators in terms of continuum energy eigenstates,

$$\delta(E-H) = \frac{1}{2\pi\hbar} \left|\psi_E\right\rangle \left\langle\psi_E\right| , \tag{7}$$

and evaluating the flux operators in the coordinate representation,

$$F = -\frac{i\hbar}{2m}\left[\frac{d}{dq}\delta(q-q^\ddagger) + \delta(q-q^\ddagger)\frac{d}{dq}\right], \tag{8}$$

one finds that $N(E)$ in Eq. (6) reduces to

$$N(E) = \frac{1}{2}\left|j_E(q^\ddagger)\right|^2, \tag{9}$$

where $j_E(q^\ddagger)$ is the steady-state (time-independent) probability density flux through the dividing surface:

$$j_E(q^\ddagger) = -\frac{i\hbar}{2m}\left[\psi_E(q^\ddagger)^* \frac{d\psi_E(q^\ddagger)}{dq^\ddagger} - \frac{d\psi_E(q^\ddagger)^*}{dq^\ddagger}\psi_E(q^\ddagger)\right]. \tag{10}$$

That this is independent of the choice of $q^\ddagger$ follows immediately from the quantum mechanical continuity equation

$$\frac{\partial}{\partial q^\ddagger} j_E(q^\ddagger) = -\frac{\partial}{\partial t}\left|\psi_E(q^\ddagger)\right|^2 = 0, \tag{11}$$

and this argument can be generalized to bimolecular reactions in any number of dimensions by noting that the steady-state flux through a closed surface is always zero as a result of the multi-dimensional generalization of Eq. (11).[7]

One final preliminary that we shall need before moving on to discuss the RPMD method[29] is to note that Eqs. (2) continue to hold when the symmetrically-thermalized time correlation functions in Eqs. (3) are replaced by their Kubo-transformed[33] analogues

$$\tilde{c}_{ff}(t) = \frac{1}{\beta}\int_0^\beta d\lambda \,\mathrm{tr}\left[e^{-(\beta-\lambda)H} F e^{-\lambda H} e^{+iHt/\hbar} F e^{-iHt/\hbar}\right], \tag{12a}$$

$$\tilde{c}_{fs}(t) = \frac{1}{\beta}\int_0^\beta d\lambda \,\mathrm{tr}\left[e^{-(\beta-\lambda)H} F e^{-\lambda H} e^{+iHt/\hbar} h e^{-iHt/\hbar}\right], \tag{12b}$$

and

$$\tilde{c}_{ss}(t) = \frac{1}{\beta}\int_0^\beta d\lambda \,\mathrm{tr}\left[e^{-(\beta-\lambda)H} h e^{-\lambda H} e^{+iHt/\hbar} h e^{-iHt/\hbar}\right]. \tag{12c}$$

This follows, for example, from the fact that the Fourier transform of $c_{ff}(t)$,

$$C_{ff}(\omega) = \int_{-\infty}^{\infty} e^{-i\omega t} c_{ff}(t)\, dt, \tag{13}$$

is related to that of $\tilde{c}_{ff}(t)$ by

$$C_{ff}(\omega) = \frac{(\beta\hbar\omega/2)}{\sinh(\beta\hbar\omega/2)}\tilde{C}_{ff}(\omega); \tag{14}$$

since the two Fourier transforms are the same in the limit as $\omega \to 0$ one can substitute either $\tilde{c}_{ff}(t)$ or $\tilde{c}_{ff}(t)$ into Eq. (2a) to obtain the same reaction rate coefficient $k(T)$. (The Kubo-transformed version of the theory[36] actually predates the symmetrically thermalized version,[34] and was obtained by an altogether different argument. However the two versions are equally valid and which one chooses to use in a particular context is simply a matter of convenience.[37])

B. Ring polymer molecular dynamics

The RPMD method is based on the Kubo-transformed version[36] of reaction rate theory and begins by approximating the side-side correlation function in Eq. (12c) as[29]

$$\tilde{c}_{ss}(t) \simeq \frac{1}{(2\pi\hbar)^n}\int d\mathbf{p}_0 \int d\mathbf{q}_0\, e^{-\beta_n H_n(\mathbf{p}_0,\mathbf{q}_0)} h_n(\mathbf{q}_0) h_n(\mathbf{q}_t), \tag{15}$$

where $\beta_n = \beta/n$ with n being the number of ring-polymer[38] (imaginary time path integral) beads. The classical Hamiltonian $H_n(\mathbf{p},\mathbf{q})$ in this equation is that of a harmonic ring polymer that experiences an external potential of $V(q)$ on each bead,

$$H_n(\mathbf{p},\mathbf{q}) = \sum_{j=1}^{n}\left[\frac{p_j^2}{2m} + \frac{1}{2}m\omega_n^2(q_j - q_{j-1})^2 + V(q_j)\right], \tag{16}$$

where $\omega_n = 1/(\beta_n\hbar)$ and $q_0 = q_n$. The time-evolved ring-polymer coordinates $\mathbf{q}_t \equiv \mathbf{q}_t(\mathbf{p}_0,\mathbf{q}_0)$ in Eq. (15) are obtained from the classical dynamics generated by this Hamiltonian,

$$\dot{p}_j = -m\omega_n^2(2q_j - q_{j-1} - q_{j+1}) - \frac{dV(q_j)}{dq_j}, \tag{17}$$

$$\dot{q}_j = \frac{p_j}{m}, \tag{18}$$

and the side functions $h_n(\mathbf{q}_0)$ and $h_n(\mathbf{q}_t)$ involve an average over the beads of the polymer necklace at times 0 and t:

$$h_n(\mathbf{q}) = \frac{1}{n}\sum_{j=1}^{n} h(q_j - q^\ddagger). \tag{19}$$

The corresponding approximation to the Kubo-transformed flux-side correlation function $\tilde{c}_{fs}(t)$ can be obtained by differentiating $\tilde{c}_{ss}(t)$ with respect to time (compare Eqs. (2b) and

(2c)). Exploiting the symmetries of the classical ring-polymer dynamics and the equivalence of the ring-polymer beads, one finds that the result of this differentiation can be rearranged to the form[29]

$$\tilde{c}_{fs}(t) \simeq \frac{1}{(2\pi\hbar)^n} \int d\mathbf{p}_0 \int d\mathbf{q}_0 \, e^{-\beta_n H_n(\mathbf{p}_0,\mathbf{q}_0)} \delta_1(\mathbf{q}_0) v_1(\mathbf{p}_0) h_n(\mathbf{q}_t), \tag{20}$$

where $\delta_1(\mathbf{q}) = \delta(q_1 - q^\ddagger)$ and $v_1(\mathbf{p}) = p_1/m$. The RPMD calculation of $\tilde{c}_{fs}(t)$ therefore boils down to pinning the first bead of the ring-polymer necklace to the transition state dividing surface at time $t = 0$, and then correlating the initial velocity of this bead with the fraction of the ring polymer that lies on the product side of the dividing surface at time t (see Fig. 1).

The approximation to $\tilde{c}_{fs}(t)$ in Eq. (20) clearly gives the correct flux-side correlation function

$$c_{fs}^{\rm cl}(t) = \frac{1}{2\pi\hbar} \int dp_0 \int dq_0 \, e^{-\beta H(p_0,q_0)} \delta(q_0 - q^\ddagger) \frac{p_0}{m} h(q_t - q^\ddagger) \tag{21}$$

in the classical ($n = 1$ bead) limit, and one can also show that it gives the exact quantum mechanical rate coefficient for the transmission through a parabolic barrier (in the limit as $n \to \infty$).[29] This "pinning" of the method to the purely classical and parabolic barrier quantum mechanical results is clearly desirable, and it probably goes a long way towards explaining why the multi-dimensional generalization of Eq. (20) has been found to work as well as it has.[29]

However, we have to admit that we did miss two crucial aspects of the theory in our earlier study.[29] The first is that Eq. (20) can be replaced by a more efficient formula that already gives a pretty good QTST approximation to the rate coefficient in the short-time limit. The second is that both Eq. (20) and this new formula, like the exact quantum mechanical correlation functions in Eq. (12), are rigorously independent of the choice of the dividing surface in the long-time limit. We shall now discuss these aspects in more detail.

C. Centroid correlation functions

The key observation that improves on our original formulation[29] is that the long-time limit of the side-side correlation function in Eq. (15) can be calculated equivalently as[39]

$$\tilde{c}_{ss}(t) \simeq \frac{1}{(2\pi\hbar)^n} \int d\mathbf{p}_0 \int d\mathbf{q}_0 \, e^{-\beta_n H_n(\mathbf{p}_0,\mathbf{q}_0)} h(\overline{q}_0 - q^\ddagger) h(\overline{q}_t - q^\ddagger), \tag{22}$$

where $h(q)$ is an ordinary Heaviside step function ($h(q) = 0$ if $q < 0$ and 1 if $q > 0$) and $\overline{q}_0$ and $\overline{q}_t$ are the centroids of the ring-polymer coordinates at times 0 and t:

$$\overline{q} = \frac{1}{n}\sum_{j=1}^{n} q_j. \tag{23}$$

It should be clear that Eqs. (15) and (22) will give the same result after an initial period that depends on the time taken for a typical ring polymer at reciprocal temperature β_n to cross the dividing surface (from the first bead to the last bead), since this is the time scale over which $h_n(\mathbf{q}_t)$ and $h(\overline{q}_t - q^\ddagger)$ differ. After this initial induction period one can equally well autocorrelate the population of ring-polymer centroids on the product side of the dividing surface [Eq. (22)] as the average population of the ring-polymer beads [Eq. (15)].

Proceeding as before and differentiating Eq. (22) with respect to time, we obtain the following approximation to the flux-side correlation function $\tilde{c}_{fs}(t)$,

$$\tilde{c}_{fs}(t) \simeq \frac{1}{(2\pi\hbar)^n}\int d\mathbf{p}_0 \int d\mathbf{q}_0\, e^{-\beta_n H_n(\mathbf{p}_0,\mathbf{q}_0)}\delta(\overline{q}_0 - q^\ddagger)\frac{\overline{p}_0}{m}h(\overline{q}_t - q^\ddagger), \tag{24}$$

where $\overline{p}_0$ is the centre-of-mass momentum of the ring polymer at time $t = 0$:

$$\overline{p} = \frac{1}{n}\sum_{j=1}^{n} p_j. \tag{25}$$

Equation (24) is the central result of this paper, and its interpretation is therefore sketched in Fig. 2. Rather than pinning the first bead of the ring polymer to the dividing surface at $t = 0$ as in Fig. 1, the centroid of the polymer is now pinned to the dividing surface, and the initial velocity factor is $\overline{p}/m$ instead of p_1/m. This is then correlated with the projection of the ring-polymer centroid on the product side of the dividing surface at time t.

D. A symmetric Eckart barrier

Although Eq. (24) has the same long-time limit as Eq. (20) and therefore gives the same reaction rate [see Eq. (2b)], it is numerically a great deal more convenient. We shall now illustrate this with some calculations on a simple Eckart barrier

$$V(q) = \frac{V_0}{\cosh^2(q/a)}, \tag{26}$$

with parameters chosen to model the gas phase H+H_2 reaction ($m = 1061\, m_e$, $V_0 = 0.425$ eV and $a = 0.734$ bohr). With these parameters $n = 128$ ring-polymer beads suffice to give well converged results down to a temperature of 200 K.

First of all, to demonstrate that Eq. (24) does indeed give the same rate as Eq. (20), we have plotted in Fig. 3 the flux-side correlation functions of the two equations as a function of time for temperatures of 300 and 1000 K. In this figure, the dividing surface has been located at the transition state ($q^{\ddagger} = 0$), and both flux-side correlation functions have been divided by the reactant partition function $Q_r(T) = (m/2\pi\beta\hbar^2)^{1/2}$ to give a quantity that tends to the rate coefficient in the long-time limit. One sees from the figure that while the correlation function in Eq. (20) takes on the order of 10 fs to reach this limit at both temperatures, the correlation function in Eq. (24) gives the same result almost instantly, and is therefore far superior from a numerical point of view. We shall return to explain why Eq. (24) gives the rate so efficiently for this problem in a moment.

The second numerical advantage of Eq. (24) over Eq. (20) is that the statistics of the integral over the initial ring-polymer phase space are far better in the former equation. The reason for this is illustrated in Fig. 4, which compares the factor

$$f_1(\mathbf{p},\mathbf{q}) = \frac{p_1}{m} e^{-\beta_n \sum_{j=1}^{n} V(q_j)} \tag{27}$$

that contributes to the integrand of Eq. (20) at time zero with the corresponding factor

$$\overline{f}(\mathbf{p},\mathbf{q}) = \frac{\overline{p}}{m} e^{-\beta_n \sum_{j=1}^{n} V(q_j)} \tag{28}$$

in the integrand of Eq. (24). In each case, the values of $f(\mathbf{p},\mathbf{q})$ are shown as histograms over the trajectories that end up on the product side of the dividing surface in the long time limit and so make a contribution to the reaction rate. The temperature in the figure is 300 K and the dividing surface has again been placed at $q^{\ddagger} = 0$.

One sees from the top panel of Fig. 4 that there is a great deal of cancellation between positive and negative contributions to the integral over the initial phase space when the rate is calculated using Eq. (20). This clearly arises because ring polymers in which the first bead has a negative velocity along the reaction coordinate at $t = 0$ can end up on the product side of the dividing surface in the long-time limit (see Fig. 1). However, it is much less likely that a ring polymer will end up on the product side at long times if its centre-of-mass velocity $\overline{p}/m$ is initially negative and the dividing surface is in an appropriate place (see Fig. 2). There is consequently hardly any cancellation between positive and negative contributions to the integral over the initial phase space for a symmetric Eckart barrier when the rate is calculated using Eq. (24).

It should be clear from Fig. 4 that the statistics of a Monte Carlo evaluation of the integral in Eq. (24) will be far better than those of an evaluation of the integral in Eq. (20). Because of these improved statistics, 10^5 ring-polymer trajectories are sufficient to give a fully converged rate coefficient at 300 K using Eq. (24), whereas 10^7 are required in Eq. (20). Since the centroid flux-side correlation function also gives the reaction rate almost instantly for a symmetric Eckart barrier (provided the dividing surface is chosen in the right place – see Fig. 3), it is clear that this new formulation of the problem is significantly more efficient than the one we presented before.[29] The fundamental reason for this is that the new formulation pins the initial ring polymer more tightly to the transition state dividing surface and is therefore closer in spirit to what is known to be one of the most efficient ways of computing a classical reaction rate.[40–43] We shall therefore abandon Eq. (20) from this point on and concentrate exclusively on Eq. (24).

Finally, for the record, Fig. 5 shows how the rate calculated using this equation compares with the exact quantum mechanical result over a temperature range extending from 200 to 2000 K. The upper panel of the figure shows the comparison on an Arrhenuis plot and the lower panel shows the percentage error in the RPMD rate as a function of $1/T$. One sees from this figure, as we did previously using our earlier formulation,[29] that the RPMD approximation gives a rate that becomes exact in the classical (high temperature) limit and that differs from the exact quantum mechanical result by less than 50% in the deep quantum tunneling regime. This is at least as good as the performance of the classical Wigner model for this problem,[44] and comparable to the performance of the simplest (single dividing surface) implementation of the QI model.[21]

E. The short time limit

Let us now return to examine the short-time limit of Eq. (24) and explain why this limit already gives an excellent approximation to the final RPMD reaction rate for a symmetric Eckart barrier when $q^\ddagger$ is located at the transition state (see Fig. 3).

As t approaches zero from above, the product side function $h(\overline{q}_t - q^\ddagger)$ in Eq. (24) can clearly be replaced by $h(\overline{p}_0)$, which allows one to separate the integrals over the ring polymer coordinates and momenta:

$$\tilde{c}_{fs}(t \to 0_+) \simeq \frac{I_p^{(n)} I_q^{(n)}}{(2\pi\hbar)^n}, \tag{29}$$

where

$$I_p^{(n)} = \int dp_1 \ldots \int dp_n \, \frac{\overline{p}}{m} h(\overline{p}) e^{-\beta_n \sum_{j=1}^{n} p_j^2/2m}, \tag{30}$$

and

$$I_q^{(n)} = \int dq_1 \ldots \int dq_n \, \delta(\overline{q} - q^{\ddagger}) e^{-\beta_n \sum_{j=1}^{n} \left[m\omega_n^2 (q_j - q_{j-1})^2/2 + V(q_j) \right]}, \tag{31}$$

with $\overline{p}$ defined in Eq. (25) and $\overline{q}$ in Eq. (23).

The integral over the momenta can be evaluated in a straightforward way to give

$$I_p^{(n)} = \left(\frac{1}{2\pi m \beta} \right)^{1/2} \left(\frac{2\pi m}{\beta_n} \right)^{n/2}, \tag{32}$$

the first factor in which will be recognized as a purely classical estimate of the reactive flux at the transition state:

$$\frac{1}{2} \langle |\dot{q}| \rangle_{\rm cl} = \left(\frac{1}{2\pi m \beta} \right)^{1/2}. \tag{33}$$

Furthermore, it is clear from a Trotter discretization of the cyclic path integral that $I_q^{(n)}$ will become proportional to a centroid-constrained partition function[8–10] in the large n limit:

$$\lim_{n \to \infty} \left(\frac{m}{2\pi \beta_n \hbar^2} \right)^{n/2} I_q^{(n)} = Q(q^{\ddagger}), \tag{34}$$

where

$$Q(q^{\ddagger}) = \oint Dq(\tau) \delta(\overline{q} - q^{\ddagger}) e^{-S[q(\tau)]/\hbar}, \tag{35}$$

with

$$S[q(\tau)] = \int_0^{\beta\hbar} d\tau \left\{ \frac{1}{2} m \dot{q}(\tau)^2 + V[q(\tau)] \right\}, \tag{36}$$

and

$$\overline{q} = \frac{1}{\beta\hbar} \int_0^{\beta\hbar} q(\tau) d\tau. \tag{37}$$

Combining these two results gives

$$\tilde{c}_{fs}(t \to 0_+) \simeq \frac{1}{2} \langle |\dot{q}| \rangle_{\rm cl} \, Q(q^{\ddagger}), \tag{38}$$

which when divided by the reactant partition function $Q_r(T)$ will be recognized as providing a primitive "quantum transition state theory" approximation to the reaction rate coefficient:[10]

$$k^{\rm QTST}(T) = \frac{1}{Q_r(T)} \tilde{c}_{fs}(t \to 0_+) = \frac{1}{2} \langle |\dot{q}| \rangle_{\rm cl} \, Q(q^{\ddagger}) / Q_r(T). \tag{39}$$

The RPMD flux-side correlation function in Eq. (24) therefore reduces to the early Voth-Chandler-Miller[10] version of QTST in the short-time limit. This is an appealing feature of

the method for several reasons. In particular, it means that for direct reactions in which transition state recrossing effects are unimportant the final RPMD reaction rate will be obtained almost instantly, provided the dividing surface is located in the right place. We have already demonstrated this numerically for a symmetric Eckart barrier, for which the optimum location of the dividing surface is determined by symmetry and the Voth-Chandler-Miller QTST result actually gives quite a good approximation to the exact quantum mechanical reaction rate (see Fig. 5).

F. The long time limit

It is well known, and straightforward to show by analogy with the above argument, that the purely classical expression for $c_{fs}^{\rm cl}(t)$ in Eq. (21) furnishes the classical transition state theory rate coefficient in the short-time limit:

$$k_{\rm cl}^{\rm TST}(T) = \frac{1}{Q_r(T)} c_{fs}^{\rm cl}(t \to 0_+) = \frac{1}{2} \langle |\dot{q}| \rangle \, e^{-\beta V(q^\ddagger)}. \tag{40}$$

This classical transition state theory rate is clearly dependent on the choice of the dividing surface $q^\ddagger$, which should ideally be chosen so as to minimize the computed rate[45,46] (i.e., to be located at the top of the reaction barrier). However, the exact classical rate coefficient,

$$k_{\rm cl}(T) = \frac{1}{Q_r(T)} \lim_{t\to\infty} c_{fs}^{\rm cl}(t), \tag{41}$$

like the exact quantum mechanical rate coefficient in Eq. (2), is rigorously independent of the location of the dividing surface.[7] The real-time dynamics in the exact classical rate formula [Eq. (41)] thus eliminates the deficiencies of transition state theory and gives the same rate coefficient for any choice of $q^\ddagger$.

That this is also true in the RPMD case can be seen from the following argument. A straightforward differentiation of Eq. (22) with respect to $q^\ddagger$ gives an integral involving a sum of two terms:

$$\frac{\partial \tilde{c}_{ss}(t)}{\partial q^\ddagger} = -\frac{1}{(2\pi\hbar)^n} \int d\mathbf{p}_0 \int d\mathbf{q}_0 \, e^{-\beta_n H_n(\mathbf{p}_0,\mathbf{q}_0)} \left[\delta(\overline{q}_0 - q^\ddagger) h(\overline{q}_t - q^\ddagger) + h(\overline{q}_0 - q^\ddagger) \delta(\overline{q}_t - q^\ddagger) \right]. \tag{42}$$

But in view of Liouville's theorem [$\int d\mathbf{p}_0 \int d\mathbf{q}_0 = \int d\mathbf{p}_t \int d\mathbf{q}_t$], and the fact that the classical ring polymer dynamics in Eqs. (17) and (18) conserves the Boltzmann factor $e^{-\beta_n H_n(\mathbf{p}_0,\mathbf{q}_0)}$

$[= e^{-\beta_n H_n(\mathbf{p}_t,\mathbf{q}_t)}]$, it is clear that the second of these two terms can be rewritten as

$$-\frac{1}{(2\pi\hbar)^n}\int d\mathbf{p}_0 \int d\mathbf{q}_0\, e^{-\beta_n H_n(\mathbf{p}_0,\mathbf{q}_0)} h(\overline{q}_{-t} - q^\ddagger)\delta(\overline{q}_0 - q^\ddagger). \tag{43}$$

So by exploiting the time-reversal symmetry of the ring polymer dynamics $[\overline{q}_{-t}(\mathbf{p}_0,\mathbf{q}_0) = \overline{q}_t(-\mathbf{p}_0,\mathbf{q}_0)]$ and the fact that $e^{-\beta_n H_n(-\mathbf{p}_0,\mathbf{q}_0)} = e^{-\beta_n H_n(\mathbf{p}_0,\mathbf{q}_0)}$, we find that this second term is the same as the first:

$$\frac{\partial \tilde{c}_{ss}(t)}{\partial q^\ddagger} = -\frac{2}{(2\pi\hbar)^n}\int d\mathbf{p}_0 \int d\mathbf{q}_0\, e^{-\beta_n H_n(\mathbf{p}_0,\mathbf{q}_0)} \delta(\overline{q}_0 - q^\ddagger) h(\overline{q}_t - q^\ddagger). \tag{44}$$

And since $\tilde{c}_{fs}(t)$ is minus the time derivative of $\tilde{c}_{ss}(t)$, we can now use Eq. (44) to calculate the derivative of the RPMD flux-side correlation with respect to the location of the dividing surface:

$$\frac{\partial \tilde{c}_{fs}(t)}{\partial q^\ddagger} = \frac{2}{(2\pi\hbar)^n}\int d\mathbf{p}_0 \int d\mathbf{q}_0\, e^{-\beta_n H_n(\mathbf{p}_0,\mathbf{q}_0)} \delta(\overline{q}_0 - q^\ddagger) \delta(\overline{q}_t - q^\ddagger) \frac{\overline{p}_t}{m}. \tag{45}$$

It should be clear from this result that $\partial \tilde{c}_{fs}(t)/\partial q^\ddagger$ will be zero unless one or more ring-polymer trajectory has a centroid that (i) starts out at $q^\ddagger$ at $t = 0$, (ii) returns to $q^\ddagger$ at time t, and (iii) has a non-zero velocity $\overline{p}_t/m$ along the reaction coordinate at time t. For a general time t, there is no reason why all three of these conditions should not be satisfied, and so $\tilde{c}_{fs}(t)$ will in general depend on the location of the dividing surface. However, conditions (ii) and (iii) are clearly incompatible in the limit as $t \to \infty$. The converged RPMD rate coefficient

$$k(T) = \frac{1}{Q_r(T)} \lim_{t\to\infty} \tilde{c}_{fs}(t) \tag{46}$$

thus has a zero first derivative with respect to $q^\ddagger$ (for all $q^\ddagger$), and it is therefore rigorously independent of the location of the dividing surface.

This (crucial) result is illustrated in Fig. 6 for the symmetric Eckart barrier that we considered in Section II.D. The top panel of the figure shows the location of five separate dividing surfaces on this potential: the optimum transition state dividing surface at the barrier maximum, two surfaces located where the potential has half its maximum value, and two further surfaces located twice as far out. The middle panel shows the flux-side correlation function in Eq. (24) as a function of time for each of these dividing surfaces at a temperature of 300 K. The bottom panel compares the final ($t \to \infty$) RPMD reaction rate at this temperature with the initial ($t \to 0_+$) QTST rate as a function of the location of the dividing surface.

The results in Fig. 6 speak for themselves. The QTST rate is extremely sensitive to the location of the dividing surface and changes by nearly six orders of magnitude over the range of the figure. The only location of $q^\ddagger$ for which QTST gives an accurate result is the top of the barrier ($q^\ddagger = 0$), which minimizes the QTST rate in accordance with the quantum analogue[37] of Wigner's variational principle.[45,46] However, the final RPMD rate is independent of the location of the dividing surface, and it agrees to graphical accuracy with the variationally optimum QTST rate for this problem no matter where the dividing surface is placed.

The fundamental reason for this is that the dynamics in RPMD is consistent with the statistics in the sense that it conserves both the ring-polymer phase space volume and the ring-polymer Hamiltonian $H_n(\mathbf{p},\mathbf{q})$. Thus there is an analogue of the continuity equation in quantum mechanics and Liouville's theorem in classical mechanics that enables the real-time RPMD dynamics to correct for a bad choice of dividing surface in much the same way as happens in the exact quantum mechanical [Eq. (2)] and classical [Eq. (41)] reaction rate theories.

G. An asymmetric Eckart barrier

An even more compelling demonstration of the advantage of the RPMD rate over that given by QTST is provided by calculations on an asymmetric Eckart barrier

$$V(q) = \frac{A}{1+e^{-2q/a}} + \frac{B}{\cosh^2(q/a)}, \tag{47}$$

with the following set of parameters in natural ($\hbar = k_\mathrm{B} = m = 1$) units:[16,18] $A = -18/\pi$, $B = 13.5/\pi$, and $a = 8/\sqrt{3\pi}$. The best location of the transition state dividing surface for this problem is no longer determined by symmetry, and even when this location is variationally optimized the primitive Voth-Chandler-Miller QTST expression for the rate coefficient [Eq. (39)] is found significantly to over-estimate the exact quantum mechanical rate coefficient at low temperatures.[18]

The fact that the QTST rate is again strongly dependent upon the choice of $q^\ddagger$ for this potential is illustrated in Fig. 7, which shows the logarithm of the transmission coefficient

$$\kappa = \frac{k(T)}{k_\mathrm{cl}(T)} \tag{48}$$

calculated by the QTST ($t \to 0_+$) and RPMD ($t \to \infty$) methods as a function of $q^\ddagger$ in the range $-3 \leq q^\ddagger \leq 0$, for reciprocal temperatures of $\beta = 4$, 8 and 12. While the QTST rate varies by nearly five orders of magnitude over this range of $q^\ddagger$ at the lowest of these temperatures ($\beta = 12$), the RPMD rate is again independent of $q^\ddagger$ as it was for the symmetric Eckart barrier (Fig. 6). Note also from the figure that the optimum location of the dividing surface in the QTST method is in this case temperature-dependent, shifting from the top of the classical barrier [$q^\ddagger = -(a/2)\ln(2)$] in the high-temperature limit out towards the (higher) reactant asymptote at lower temperatures.

The most important observation from Fig. 7 is that, unlike the situation for the symmetric barrier, the RPMD rate is significantly lower than the variational QTST rate for the asymmetric Eckart barrier in the low temperature (deep quantum tunneling) regime. The reason for this is shown in Fig. 8, which plots the time-dependent transmission coefficient

$$\kappa(t) = \frac{\tilde{c}_{fs}(t)}{Q_r(T)k_{\rm cl}(T)} \tag{49}$$

obtained in the RPMD calculation using the optimum location of the QTST dividing surface at each temperature ($\beta = 4$, 8 and 12). For the asymmetric Eckart barrier, the RPMD dynamics predicts a significant recrossing of this transition state dividing surface at low temperatures. Note that this is a purely quantum mechanical effect, since there can be no recrossing of the optimum transition state dividing surface (the top of the barrier) for a one-dimensional reaction in classical mechanics.

As a result of the recrossing dynamics, the final RPMD transmission coefficient is in significantly better agreement with the exact quantum mechanical transmission coefficient for the asymmetric Eckart barrier than it is with the result given by QTST. This is demonstrated in Table I, which compares all three transmission coefficients with those obtained in two earlier attempts[16,47] to improve on the primitive Voth-Chandler-Miller[10] version of QTST [Eq. (39)]. In this table, the QTST and RPMD results were obtained using $n = 256$ ring-polymer beads, and the location of the dividing surface was variationally optimized at each temperature in QTST.

One sees from the table that the RPMD method does almost as well for the asymmetric Eckart barrier as it does for the symmetric barrier, giving a transmission coefficient that agrees with the exact result to within around 60% in the deep quantum tunneling regime (where $\kappa_{\rm QM}$ is greater than 4000 and $\kappa_{\rm QTST}$ is in error by a factor of around 4). One also

sees that RPMD does somewhat better than the earlier attempts of Cao and Voth[47] and Pollak and Liao[16] to improve on the original Voth-Chandler-Miller formulation[10] of QTST.

H. Multi-dimensional generalization

The appropriate generalization of Eq. (20) for a multi-dimensional reaction has already been given (and applied to a standard model for a chemical reaction in solution[48,49]) in our earlier paper.[29] However, the correct way to generalize Eq. (24) has not yet been written down. Since this new flux-side correlation function has distinct computational advantages over that in Eq. (20) we shall now end this theory section by giving this generalization here.

Consider an f-dimensional reactive system with a Hamiltonian of the form

$$H = \sum_{i=1}^{f} \frac{p_i^2}{2m_i} + V(q_1, \ldots, q_f), \tag{50}$$

and with a dividing surface $s(q_1, \ldots, q_f) = 0$ between the reactants and products such that the products are in $s > 0$. For this system, the appropriate generalization of Eq. (24) is

$$\tilde{c}_{fs}(t) \simeq \frac{1}{(2\pi\hbar)^{nf}} \int d\mathbf{p}_0 \int d\mathbf{q}_0 \, e^{-\beta_n H_n(\mathbf{p}_0, \mathbf{q}_0)} \delta[\overline{s}(\mathbf{q}_0)] \overline{v}_s(\mathbf{p}_0, \mathbf{q}_0) h[\overline{s}(\mathbf{q}_t)], \tag{51}$$

where $H_n(\mathbf{p}, \mathbf{q})$ is the classical Hamiltonian of a multi-dimensional harmonic ring polymer with an external potential of $V(q_1, \ldots, q_f)$ on each polymer bead,

$$H_n(\mathbf{p}, \mathbf{q}) = \sum_{i=1}^{f} \sum_{j=1}^{n} \left[\frac{p_{i,j}^2}{2m_i} + \frac{1}{2} m_i \omega_n^2 (q_{i,j} - q_{i,j-1})^2 \right] + \sum_{j=1}^{n} V(q_{1,j}, \ldots, q_{f,j}), \tag{52}$$

subject to the cyclic boundary condition $q_{i,0} = q_{i,n}$. The time-evolved ring-polymer coordinates $\mathbf{q}_t \equiv \mathbf{q}_t(\mathbf{p}_0, \mathbf{q}_0)$ in Eq. (51) are obtained from the dynamics generated by this Hamiltonian,

$$\dot{p}_{i,j} = -m_i \omega_n^2 (2q_{i,j} - q_{i,j-1} - q_{i,j+1}) - \frac{\partial V(q_{1,j}, \ldots, q_{f,j})}{\partial q_{i,j}}, \tag{53}$$

and

$$\dot{q}_{i,j} = \frac{p_{i,j}}{m_i}, \tag{54}$$

and the remaining quantities in the equation are defined as follows:

$$\overline{s}(\mathbf{q}) = s(\overline{q}_1, \ldots, \overline{q}_f), \tag{55}$$

with

$$\overline{q}_i = \frac{1}{n} \sum_{j=1}^{n} q_{i,j}, \tag{56}$$

and

$$\overline{v}_s(\mathbf{p},\mathbf{q}) = \sum_{i=1}^{f} \frac{\partial s(\overline{q}_1,\ldots,\overline{q}_f)}{\partial \overline{q}_i} \frac{\overline{p}_i}{m_i}, \tag{57}$$

with

$$\overline{p}_i = \frac{1}{n}\sum_{j=1}^{n} p_{i,j}. \tag{58}$$

Notice in particular that these quantities include the centroid $\overline{q}_i$ of the ring polymer in each degree of freedom and the corresponding velocity $\overline{p}_i/m_i$, and that Eq. (51) reduces correctly to Eq. (24) when $f = 1$ and $s(q) = q - q^{\ddagger}$. Notice also that Eq. (51) has the form of a purely classical flux-side correlation function in an extended ($2nf$-dimensional) phase space, with the dividing surface given in Eq. (55). Since a classical reaction rate is rigorously independent of the choice of dividing surface as a result of Liouville's theorem,[7] the same must clearly be true of the present RPMD reaction rate.

Having said this, we should stress that for a truly complex reaction it will be impractical to calculate the rate using Eq. (51) *unless* the dividing surface is chosen wisely. This is true because there will be significant recrossing of a poorly chosen dividing surface, which will make the collection of statistics difficult for reasons analogous to those illustrated in Fig. 4. Although Eq. (51) must formally give the same rate for any choice of dividing surface, the result will only be easy to obtain numerically if the recrossing is not too significant. A sensible strategy for truly complex reactions would therefore be to choose the dividing surface so as to minimize the QTST rate, and then use this variationally optimum dividing surface in a subsequent RPMD calculation. In cases where the variationally optimum QTST dividing surface is itself difficult to determine, one could even imagine using transition path sampling[50] of RPMD to determine the rate. The key point is that, since Eq. (51) has the form of a purely classical flux-side correlation function in an extended phase space, the full machinery that has been developed over the years for calculating classical reaction rates can immediately be applied to the equation.

III. SUMMARY

In this paper, we have presented a more efficient formulation of RPMD reaction rate theory[29] that focusses on the side functions of the ring-polymer centroids rather than the side functions of the individual ring-polymer beads. This leads to improved statistics in the

Monte Carlo integration over the initial ring-polymer phase space and results in a flux-side correlation function that converges more rapidly to its limiting long-time value. Indeed we have shown that this new flux-side correlation function already gives a primitive (Voth-Chandler-Miller[10]) QTST approximation to the rate coefficient in the short-time limit. More importantly, we have shown that the long-time limit of the correlation function, and hence the RPMD reaction rate, is rigorously independent of the location of the dividing surface. It will be interesting in future work to explore how well the multi-dimensional generalization of the theory in Section II.H does for more complicated reactions than the simple one-dimensional model problems we have considered here.

Acknowledgments

We would like to thank David Chandler for suggesting Eq. (22) and Bill Miller for some stimulating discussions. This work was supported by the US Office of Naval Research under contract number N000140510460.

1. J. Cao and G. A. Voth, J. Chem. Phys. **100**, 5106 (1994).
2. J. Cao and G. A. Voth, J. Chem. Phys. **101**, 6157 (1994).
3. D. R. Reichman, P.-N. Roy, S. Jang and G. A. Voth, J. Chem. Phys. **113**, 919 (2000).
4. E. Geva, Q. Shi and G. A. Voth, J. Chem. Phys. **115**, 9209 (2001).
5. Q. Shi and E. Geva, J. Chem. Phys. **116**, 3223 (2002).
6. H. Wang, X. Sun and W. H. Miller, J. Chem. Phys. **108**, 9726 (1998).
7. W. H. Miller, J. Chem. Phys. **61**, 1823 (1974).
8. M. J. Gillan, Phys. Rev. Lett. **58**, 563 (1987).
9. M. J. Gillan, J. Phys. C **20**, 3621 (1987).
10. G. A. Voth, D. Chandler and W. H. Miller, J. Chem. Phys. **91**, 7749 (1989).
11. G. A. Voth, Chem. Phys. Lett. **170**, 289 (1990).

12. R. P. McRae, G. K. Schenter, B. C. Garrett, G. R. Haynes, G. A. Voth and G. C. Schatz, J. Chem. Phys. **97**, 7392 (1992).

13. G. A. Voth, J. Phys. Chem. **97**, 8365 (1993).

14. G. A. Voth, Adv. Chem. Phys. **93**, 135 (1996).

15. N. Fisher and H. C. Andersen, J. Phys. Chem. **100**, 1137 (1996).

16. E. Pollak and J-L. Liao, J. Chem. Phys. **108**, 2733 (1998).

17. J. Shao, J-L. Liao and E. Pollak, J. Chem. Phys. **108**, 9711 (1998).

18. S. Jang and G. A. Voth, J. Chem. Phys. **112**, 8747 (2000).

19. J-L. Liao and E. Pollak, Chem. Phys. **268**, 295 (2001).

20. W. H. Miller, Y. Zhao, M. Ceotto and S. Yang, J. Chem. Phys. **119**, 1329 (2003).

21. C. Venkataraman and W. H. Miller, J. Phys. Chem. A **108**, 3035 (2004).

22. T. Yamamoto and W. H. Miller, J. Chem. Phys. **120**, 3086 (2004).

23. Y. Zhao, T. Yamamoto and W. H. Miller, J. Chem. Phys. **120**, 3100 (2004).

24. M. Ceotto and W. H. Miller, J. Chem. Phys. **120**, 6356 (2004).

25. T. Yamamoto and W. H. Miller, J. Chem. Phys. **122**, 044106 (2005).

26. M. Ceotto, S. Yang and W. H. Miller, J. Chem. Phys. **122**, 044109 (2005).

27. This is almost certainly the case in classical mechanics. However, in quantum mechanics, which does not have such a rigorous transition state theory limit, it is less clear that recrossing effects will be entirely negligible. For example, Fig. 8 shows that there is significant recrossing of the optimum Voth-Chandler-Miller QTST dividing surface even for a simple asymmetric Eckart barrier at low temperatures.

28. I. R. Craig and D. E. Manolopoulos, J. Chem. Phys. **121**, 3368 (2004).

29. I. R. Craig and D. E. Manolopoulos, J. Chem. Phys. **122**, 084106 (2005).

30. T. F. Miller III and D. E. Manolopoulos, J. Chem. Phys. **122**, 184503 (2005).

31. I. R. Craig and D. E. Manolopoulos, Chem. Phys. (in press).

32. M. Parrinello and A. Rahman, J. Chem. Phys. **80**, 860 (1984).

33. R. Kubo, J. Phys. Soc. Japan **12**, 570 (1957).

34. W. H. Miller, S. D. Schwartz and J. W. Tromp, J. Chem. Phys. **79**, 4889 (1983).

35. W. H. Miller, J. Chem. Phys. **63**, 1166 (1975).

36. T. Yamamoto, J. Chem. Phys. **33**, 281 (1960).

37. C. Predescu and W. H. Miller, J. Phys. Chem. B **109**, 6491 (2005).

38. D. Chandler and P. G. Wolynes, J. Chem. Phys. **74**, 4078 (1981).

39. D. Chandler, private communication (2004).

40. J. C. Keck, J. Chem. Phys. **32**, 1035 (1960).

41. J. C. Keck, Adv. Chem. Phys. **13**, 85 (1967).

42. C. H. Bennett, in *Algorithms for Chemical Computations*, ACS Symposium Series No. 46, edited by R. E. Christoffersen (American Chemical Society, Washington, 1977), p. 63.

43. D. Chandler, J. Chem. Phys. **68**, 2959 (1978).

44. T. Yamamoto, H. Wang and W. H. Miller, J. Chem. Phys. **116**, 7335 (2002).

45. E. P. Wigner, J. Chem. Phys. **5**, 720 (1937).

46. E. P. Wigner, Trans. Faraday Soc. **34**, 29 (1938).

47. J. Cao and G. A. Voth, J. Chem. Phys. **105**, 6856 (1996).

48. A. O. Caldeira and A. J. Leggett, Ann. Phys. (N.Y.) **149**, 374 (1983).

49. M. Topaler and N. Makri, J. Chem. Phys. **101**, 7500 (1994).

50. D. Chandler, in *Classical and Quantum Dynamics in Condensed Phase Simulations*, edited by B. J. Berne, G. Ciccotti and D. F. Coker (World Scientific, Singapore, 1998), p. 51.

TABLE I: Transmission coefficients for the asymmetric Eckart barrier.

β	QTST[a]	CV[b]	PL[c]	RPMD[d]	QM[e]
2	1.2	1.2	1.2	1.2	1.2
4	2.0	2.2	2.0	2.0	2.0
6	5.6	6.4	5.6	5.3	5.3
8	36	31	44	28	26
10	540	340	1100	310	250
12	16000	7600	28000	6400	4100

(a) Voth-Chandler-Miller QTST [Eq. (39)].

(b) Improved method of Cao and Voth [see Refs. 18 and 47].

(c) Alternative QTST of Pollak and Liao [Ref. 16].

(d) RPMD results from the present work [Eq. (46)].

(e) The exact quantum mechanical transmission coefficient.

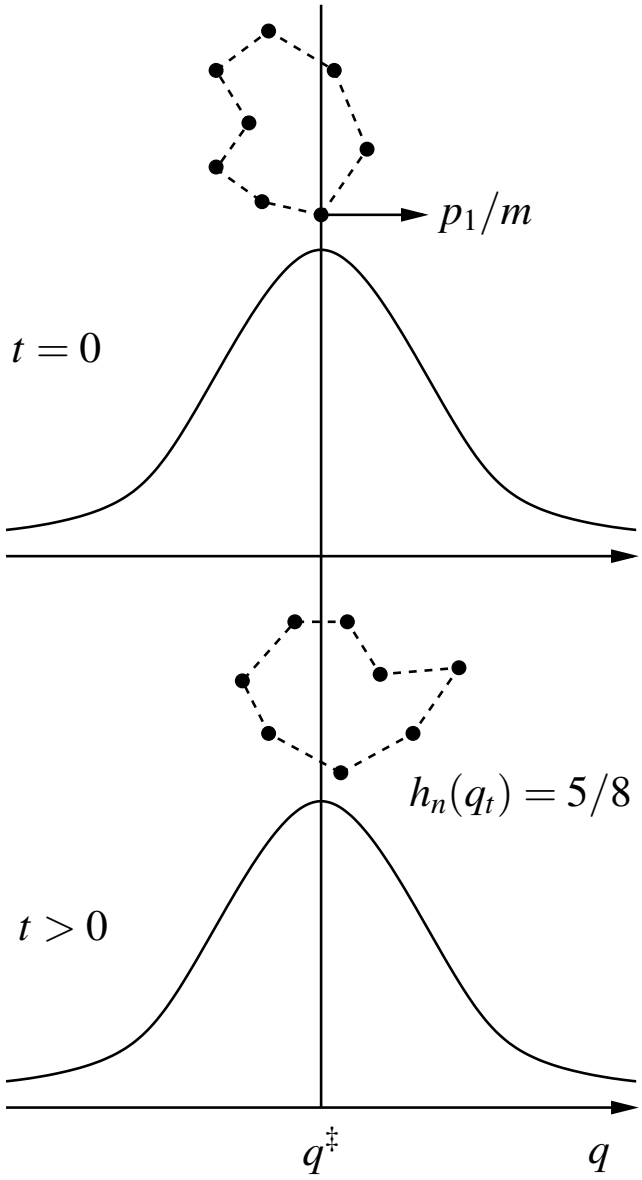

FIG. 1: Schematic illustration of the original RPMD method in Eq. (20) for calculating a reaction rate. At time zero, the first bead of the ring-polymer necklace is pinned to the transition state dividing surface, and this bead contributes a velocity factor of p_1/m to the flux-side correlation function $\tilde{c}_{fs}(t)$. The polymer then evolves under the classical equations of motion in Eqs. (17) and (18) and contributes a side factor of $h_n(\mathbf{q}_t) \in [0, 1]$ to the correlation function at time t.

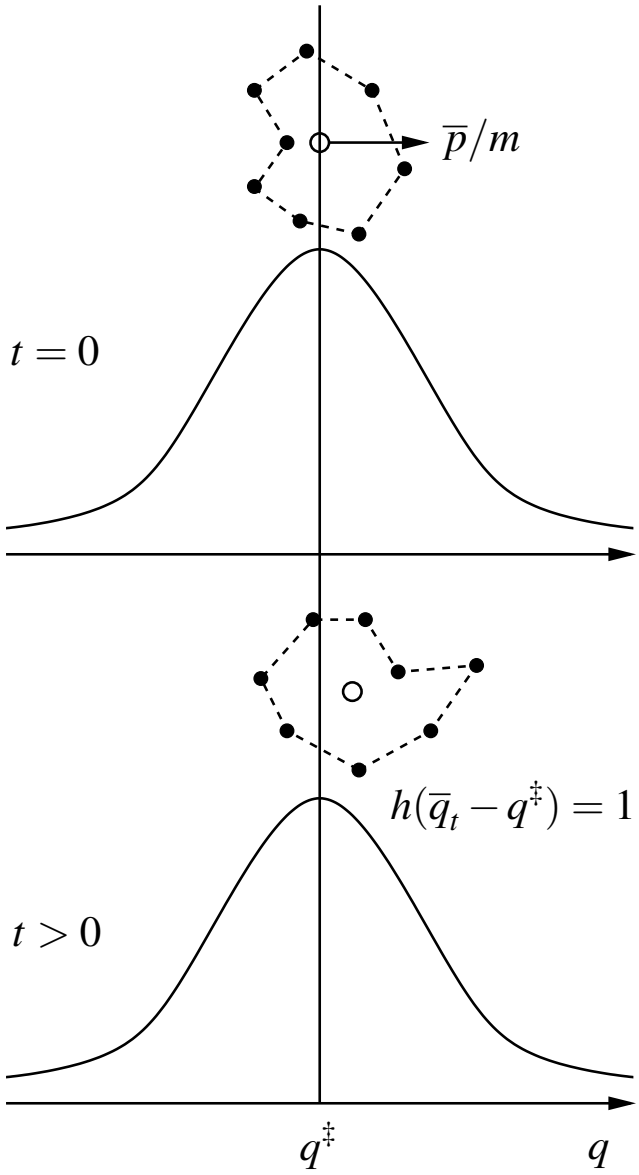

FIG. 2: Schematic illustration of the new RPMD method in Eq. (24) for calculating a reaction rate. At time zero, the centroid of the ring-polymer necklace is pinned to the transition state dividing surface, and contributes a velocity factor of $\overline{p}/m$ to the flux-side correlation function $\tilde{c}_{fs}(t)$. The polymer then evolves under the classical equations of motion in Eqs. (17) and (18) and contributes a side factor of $h(\overline{q}_t - q^{\ddagger})$ [$= 0$ or 1] to the correlation function at time t.

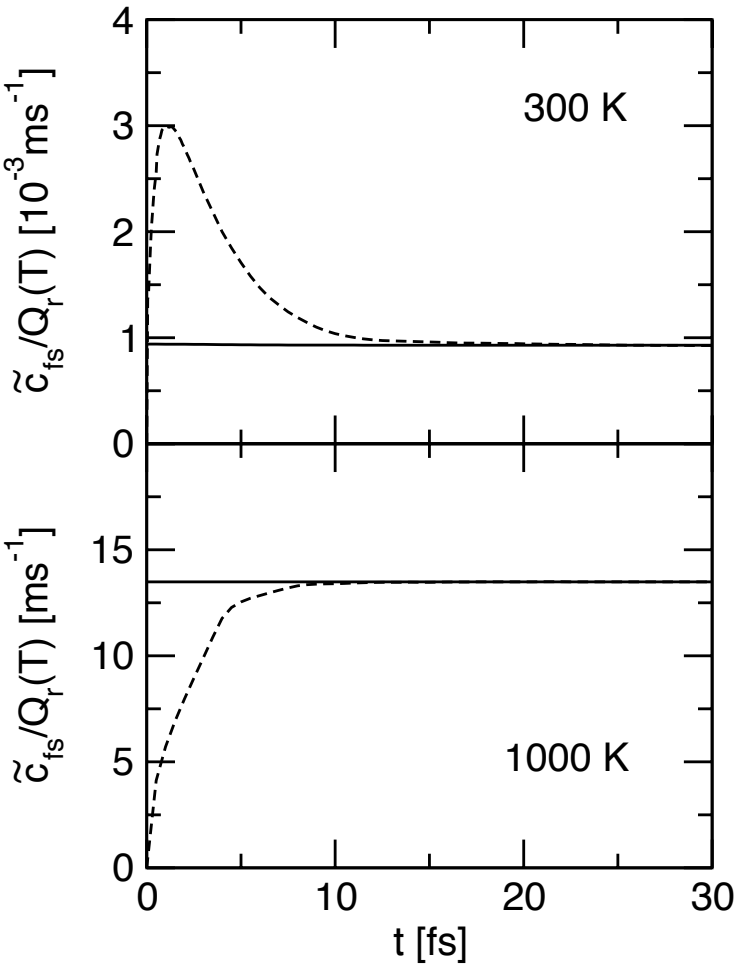

FIG. 3: Comparison of the flux-side correlation function in Eq. (24) (solid line) with that in Eq. (20) (dashed line) for the symmetric Eckart barrier at 300 and 1000 K.

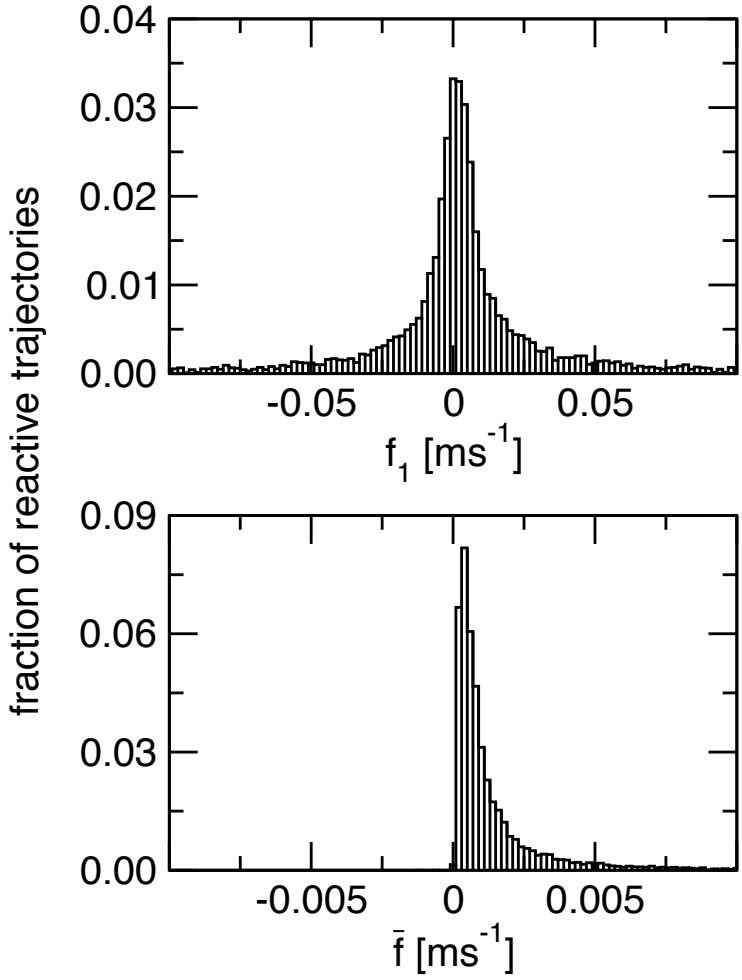

FIG. 4: Histograms of the factors $f_1(\mathbf{p},\mathbf{q})$ in Eq. (27) and $\overline{f}(\mathbf{p},\mathbf{q})$ in Eq. (28) for the symmetric Eckart barrier at 300 K.

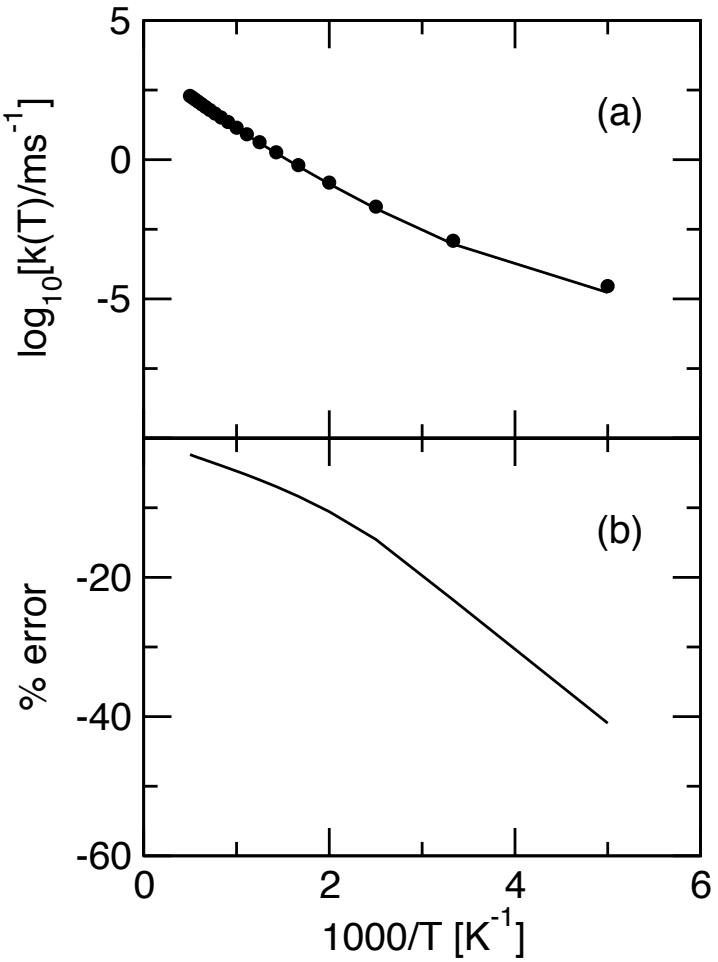

FIG. 5: (a) An Arrhenius plot of the rate coefficient for the symmetric Eckart barrier. The solid line is the RPMD result obtained from Eq. (24) and the filled circles indicate the exact quantum mechanical rate. (b) Percentage error in the RPMD result over the same temperature range as in (a).

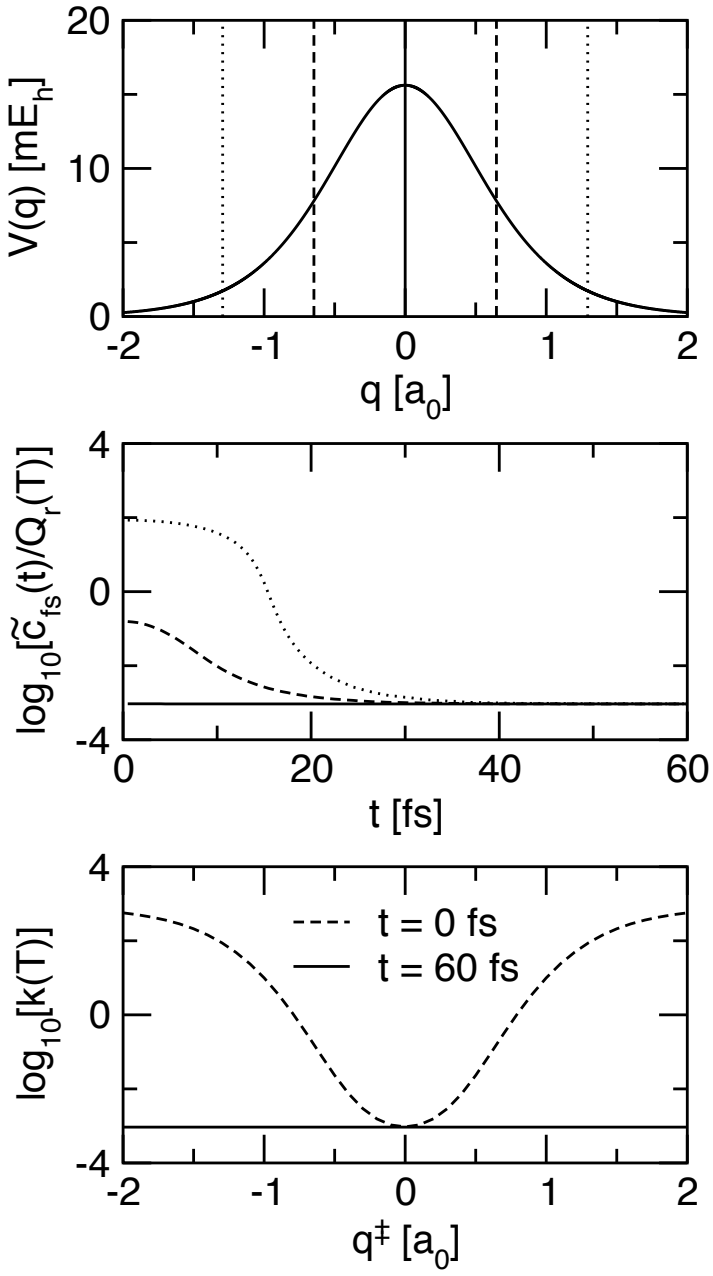

FIG. 6: Top panel: the location of five different dividing surfaces on the symmetric Eckart barrier. Middle panel: the computed RPMD flux-side correlation functions at 300 K for each of these dividing surfaces. (Note that dividing surfaces at $+q^{\ddagger}$ and $-q^{\ddagger}$ give the same correlation functions by symmetry.) Bottom panel: dependence of the QTST ($t \to 0$) and RPMD ($t \to \infty$) rate coefficients on the location of the dividing surface.

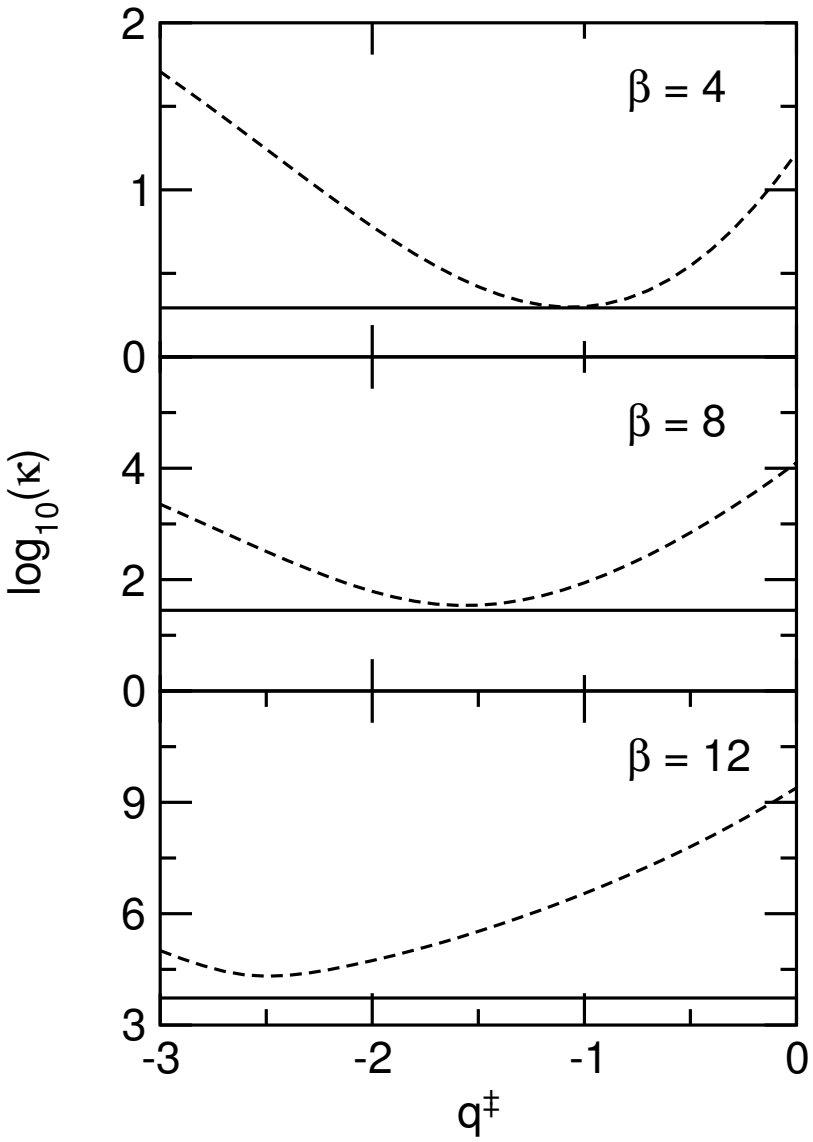

FIG. 7: Computed QTST (dashed line) and RPMD (solid line) transmission coefficients for the asymmetric Eckart barrier at three different temperatures, as a function of the location of the dividing surface $q^{\ddagger}$.

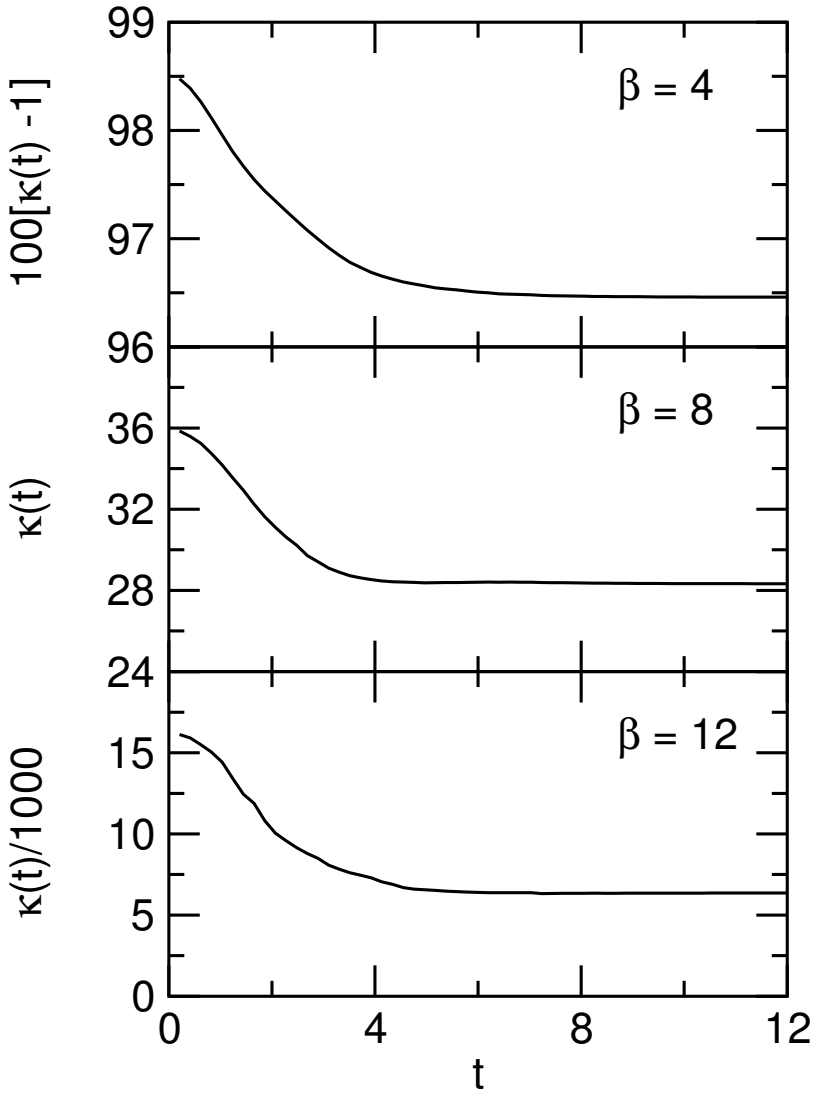

FIG. 8: Time-dependent RPMD transmission coefficients for the asymmetric Eckart barrier at the three different temperatures considered in Fig. 7.